Separator current sheets: Generic features in minimum-energy magnetic fields subject to flux constraints

D.W. Longcope

August 2, 2001

Abstract

Equations are found for force-free magnetic equilibria in the "coronal half-space" $z > 0$, subject to boundary conditions on the normal magnetic field at at $z = 0$. The distribution of normal field is assumed to be composed of N_S isolated unipolar source regions of arbitrary shape, arranged arbitrarily on the plane. The equilibria are found by minimizing the magnetic energy subject to constraints on the total flux interconnecting pairs of source regions. For N_S source regions interconnected in $N_{\mathcal{D}}$ ways, there are $N_c = N_{\mathcal{D}} - N_S + 1$ distinct constraints on the field. Minimization subject to these constraints leads to an N_c-dimensional space of equilibria, for given boundary data. All field-lines connecting source regions are current-free, but the equilibrium contains N_c current-sheets lying at certain interfaces. In a two-dimensional magnetic field current sheets occur at points topologically equivalent to X-type neutral points in the potential field. In a three-dimensional field current sheets occur at points topologically equivalent to separators in the potential field. The free magnetic energy is a function of the N_c fluxes used to constrain the variation.

1 Introduction

Force-free magnetic fields have proven to be extremely useful in the modeling of magnetized plasmas. The magnetic field in the solar corona is often assumed to be in equilibrium because it appears stationary on Alfveńic time-scales, and to be force-free because its plasma pressure is believed to be quite small ($\beta \sim 10^{-3}$). Coronal equilibria are often sought for a magnetic field in the half-space $z > 0$ (the corona) matching a specified normal component at the photospheric surface $z = 0$,

$$B_z(x, y, z\!=\!0) \;=\; f(x, y) \quad , \tag{1}$$

and vanishing at infinity. Routine measurements of the magnetic field vector at or near the photospheric level (magnetograms) provide a practical example of such a boundary condition.

A force-free magnetic field is that which extremizes the magnetic energy

$$W = \frac{1}{2}\int_{z>0} |\nabla \times \mathbf{A}(\mathbf{x})|^2 \, d\mathbf{x} \quad , \tag{2}$$

where $\mathbf{A}$ is the vector potential of the magnetic field: $\mathbf{B} = \nabla \times \mathbf{A}$. If the variation of $\mathbf{A}(\mathbf{x})$ is subject only to the requirement that the magnetic field match the boundary condition (1) then the solution is a potential magnetic field

$$\nabla \times (\nabla \times \mathbf{A}) = 0 \quad . \tag{3}$$

It is well known that the solution to (3) subject to boundary conditions on all is unique, and that its energy is a minimum [1].

In many cases the variation is subject to additional constraints, leading to different classes of force-free equilibria. The most restrictive constraint is that $\delta\mathbf{A}$ be consistent with the ideal induction equation,

$$\delta\mathbf{A}(\mathbf{x}) = \delta\boldsymbol{\xi} \times \mathbf{B} \quad , \tag{4}$$

for some plasma displacements $\delta\boldsymbol{\xi}(\mathbf{x})$. Demanding that the magnetic energy be stationary under arbitrary displacements $\delta\boldsymbol{\xi}$, vanishing at $z = 0$, leads to the equation for a general force-free equilibrium

$$(\nabla \times \mathbf{B}) \times \mathbf{B} = 0 \quad . \tag{5}$$

Each coronal field-line maps a photospheric point where $f(x, y) > 0$ to one where $f(x, y) < 0$ (neglecting open field-lines). Restricting the variation to ideal plasma motions prevents the perturbations from changing this mapping. Constraint (4) is thus equivalent to a *line-tying constraint* whereby the ends of every field line are fixed within the photospheric plane.

Line-tying represents a constraint on the variation, so the minimum is over a subset of all magnetic fields consistent with the boundary data. The energy of a general force-free field is therefore always greater than that of the corresponding potential field. The difference in energy between the two fields, ΔW, is called the *free-energy* since it may be released without changing the photospheric flux distribution. (Solar flares occur during a relatively short time, during which the photospheric field does not appear to change significantly [2].)

Singular magnetic equilibria have been proposed by way of explaining observed rates of energy deposition in both the quiet [3, 4] and flaring corona [5]. The current density at a tangential discontinuity in the magnetic field is formally infinite [6] which is only possible in a plasma whose resistivity is exactly zero, and therefore not directly relevant to the solar corona. Since the resistivity of the coronal plasma is extremely low, the ideal approximation is suitable everywhere except in the neighborhood of the discontinuity. It is therefore believed that ideal evolution *toward* a singular equilibrium would produce localized heating and rapid magnetic reconnection [7]. We will work in the ideal limit, and admit the possibility of a discontinuous magnetic field, recognizing that the result is not an achievable coronal field.

Examples of current sheets have been exhibited in two-dimensional magnetic equilibria, e.g. translationally invariant in x [8, 9, 10, 11]. It has further been suggested that generically three-dimensional magnetic fields will have current sheet singularities [3, 12], although, because of their inherent complexity, no examples have been found. Arguing by analogy with two-dimensional examples, several authors have predicted that three-dimensional current sheets will occur where the field line mapping is discontinuous or has extremely strong gradients [13, 14]. The present work will use a variational method to prove that this assertion for a certain class of boundary conditions $f(x, y)$.

Magnetograms show the photospheric magnetic field to be generally organized into isolated patches of strong magnetic field embedded in a relatively field-free photosphere. This is believed to reflect the confinement of field beneath the photosphere into isolated flux tubes [15]. This kind of photospheric boundary condition leads to field line mappings with many discontinuities. At least in a potential field, mapping discontinuities will occur along separatrix surfaces, which are families of field lines originating in the fan-plane of magnetic nulls [16, 17]. Following an analogy with two-dimensional fields, Longcope & Cowley[18] showed that annular current sheets, called *current ribbons*, would form at the intersections of separatrix surfaces. Based on this, a theoretical model of coronal magnetic field evolution, called the Minimum Current Corona (MCC), was developed [14].

In this work we propose a new class of constraints under which minimum-energy fields may be sought. Motivated by observations we describe the photospheric field as a collection of N_S isolated source regions. The coronal magnetic field can then be divided into $N_{\mathcal{D}}$ domains according to the positive and negative sources at the footpoints of each field line. We introduce a constraint on the *domain fluxes*, the total magnetic flux in each of the domains. This constraint is less restrictive than line-tying since footpoints are free to move within a given source region but may not switch between regions. The less restrictive domain-flux constraint is natural if the detailed line-tying within each source is irrelevant or unobservable. Furthermore, the constraints lead to a non-trivial class of three-dimensional magnetostatic equilibria in which to consider the coronal energetics. It provides a lower bound on the energy of a general force-free magnetic field arising from quasi-static evolution.

The next section explains the domain-flux constraints in more detail. The connections of the field are represented as a domain graph. This formalism shows that constraining all $N_{\mathcal{D}}$ domain fluxes requires only $N_{\mathcal{D}} - N_S + 1$ mathematical constraints on the coronal field. Each of these constraints is related to the flux through a particular closed loop in the corona.

The magnetic field whose energy is minimum subject to constraints on all domain fluxes, and to the boundary condition (1), satisfies an Euler-Lagrange equation, found using the calculus of variations. In §3 we perform this constrained variation and find that the Euler-Lagrange equation defines a magnetic field which is current-free within each domain, and has $N_{\mathcal{D}}-N_S+1$ current sheets at certain locations between domains. The locations of the current sheets corresponds to the closed loops whose coronal flux was subject to constraint. The free magnetic energy of this field is determined entirely by the flux constraints.

In §4 we show that the minimization procedure recovers known two-dimensional equilibria when a translational symmetry is assumed. In §5 we show that for a generically three-dimensional field the locations of the current sheets are topologically equivalent to the locations of separator field lines in an equivalently connected potential magnetic field. This procedure may be used to predict the locations of current sheets in the magnetic field arising from an arbitrary distribution of source regions. The free magnetic energy for each field is a function of $N_{\mathcal{D}} - N_S + 1$ fluxes.

2 The domain flux constraints

The photospheric magnetic field, $f(x, y)$, is assumed to be composed of N_S simple, distinct, isolated regions called *sources*. Each source is surrounded by unmagnetized photosphere $f = B_z = 0$. The shapes of regions and the distribution of f within them, are otherwise arbitrary. The magnetic fluxes of positive source P_i and negative source N_j are

$$\Phi_i \equiv \int\limits_{P_i} B_z(x,y)\,dx\,dy \quad , \quad \Phi_j \equiv \int\limits_{N_j} B_z(x,y)\,dx\,dy \quad , \tag{6}$$

determined by the boundary condition. Figure 1 shows an example with $N_S = 6$ sources arranged in a pattern without symmetry.

The net flux crossing the total solar surface must be zero, since there are no magnetic monopoles within the Sun. Nevertheless, it is sometimes desirable to model an unbalanced flux distribution from which open magnetic field extends. If the total flux in all sources

$$\Phi_\Sigma \equiv \sum_i \Phi_i \quad , \tag{7}$$

does not vanish, we include infinity as a single additional "source" with flux $-\Phi_\Sigma$. We will henceforth make no distinction between a source located at $z = 0$ and one at ∞, and will assume that the sum of all source-fluxes is zero.

We further assume that, with a few exceptions discussed below, each magnetic field line in the corona ($z > 0$) has the same simple topology: it begins at positive source and ends at negative source. We hereby exclude the possibility of closed or chaotic

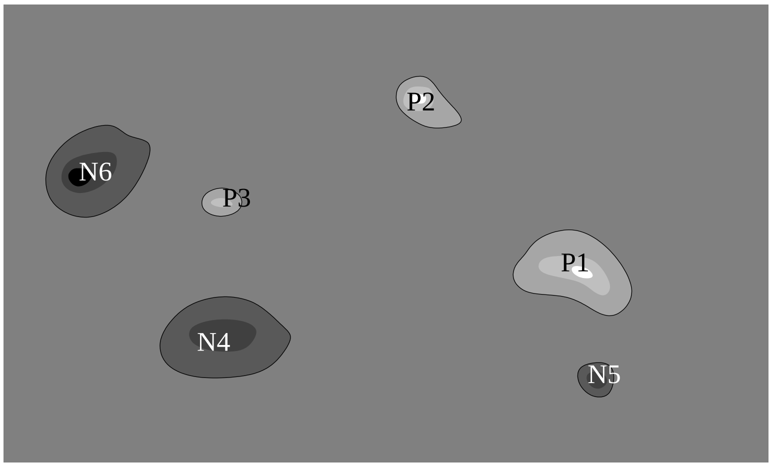

Figure 1. An example of a photospheric boundary condition, $B_z(x,y,z\!=\!0) = f(x,y)$ shown as a grey scale. The field is composed of three positive source regions P_1, P_2 and P_3 (white) and three negative source regions N_4, N_5 and N_6 (black). The unmagnetized ($f = 0$) background is grey.

magnetic field lines lying entirely above the photosphere. Under this assumption, the entire coronal volume may be partitioned into domains identified by the end-points of the field lines in each one. Domain $\mathcal{D}_{ij}$ denotes a volume in which field lines begin at source P_i and end at source N_j. The net flux in domain $\mathcal{D}_{ij}$ can be found using any surface crossed by every field line, the photosphere for example

$$\psi_{ij} \;=\; \int\limits_{P_i\cap\mathcal{D}_{ij}} B_z(x,y)\,dx\,dy \;=\; -\int\limits_{N_j\cap\mathcal{D}_{ij}} B_z(x,y)\,dx\,dy \quad . \tag{8}$$

The domain flux ψ_{ij} is defined to be a positive quantity. It is, in general, possible for a pair of sources to be connected by field lines from multiple domains. When this occurs the domains can be distinguish by with a superscript: $\mathcal{D}_{ij}^{(1)}$, $\mathcal{D}_{ij}^{(2)}$ and so on.

2.1 Connections: The domain graph

In addition to the normal field $f(x,y)$ we wish to prescribe the connections between positive and negative sources made by coronal field lines. The complete set of connections is depicted schematically through a *domain graph*, showing the sources as vertices and the domains as edges (see fig. 2). This graph defines the *connections* of the entire magnetic field, and all fields with the same domain graph are *equivalently connected*. A graph consisting of two or more separate pieces with no connections between them, is a *non-connected* graph. Such a magnetic field consists of several independent flux systems which interact with one another only through magnetic pressure. While this is an interesting problem by itself, we will restrict further consideration to connected graphs.

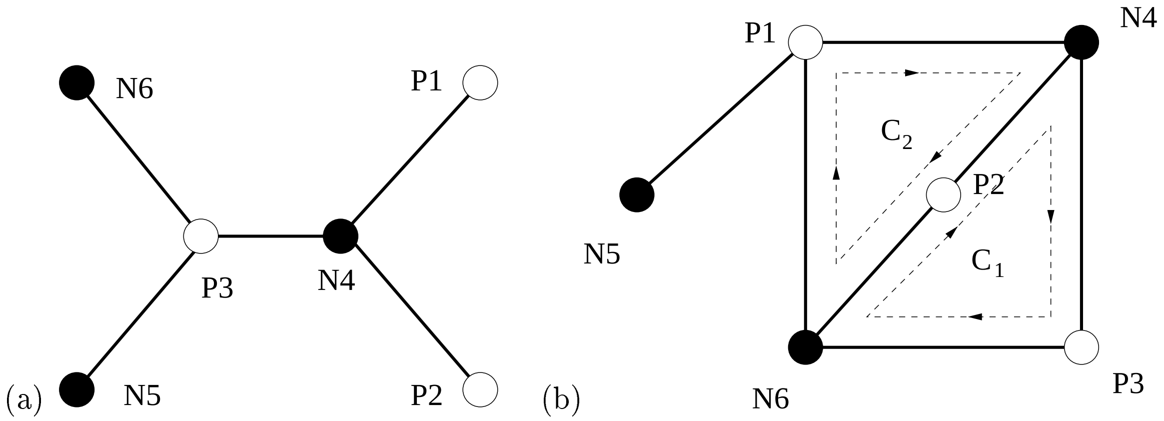

Figure 2. Two possible domain graphs for the source distribution shown in fig. 1. Graph (a) is a tree, while graph (b) contains two circuits $\mathcal{C}_1$ and $\mathcal{C}_2$ indicated with dashed lines.

A graph may be characterized by its *incidence matrix*, which has one row for each source and one column for each domain [19]. Column $\mathcal{D}_{ij}$ contains a $+1$ in the row of P_i and a -1 in the row of N_j. Forming vectors from the source fluxes Φ_i and the domain fluxes ψ_{ij} the allocation of fluxes can be expressed

$$\mathrm{A} \cdot \vec{\psi} \;=\; \vec{\Phi} \quad . \tag{9}$$

This relation relies on the assumption that every magnetic field line, except for a set of measure zero, belongs to one and only one domain.

For example, the incidence matrix for the graph in fig. 2b is

$$\mathrm{A} \;=\; \begin{array}{c} \\ P1 \\ P2 \\ P3 \\ N4 \\ N5 \\ N6 \end{array} \!\!\begin{array}{c} \begin{array}{ccccccc} \mathcal{D}_{14} & \mathcal{D}_{15} & \mathcal{D}_{16} & \mathcal{D}_{24} & \mathcal{D}_{26} & \mathcal{D}_{34} & \mathcal{D}_{36} \end{array} \\ \left(\begin{array}{ccccccc} 1 & 1 & 1 & 0 & 0 & 0 & 0 \\ 0 & 0 & 0 & 1 & 1 & 0 & 0 \\ 0 & 0 & 0 & 0 & 0 & 1 & 1 \\ -1 & 0 & 0 & -1 & 0 & -1 & 0 \\ 0 & -1 & 0 & 0 & 0 & 0 & 0 \\ 0 & 0 & -1 & 0 & -1 & 0 & -1 \end{array} \right) \end{array} \quad . \tag{10}$$

It provides the explicit relation between domain fluxes and source fluxes

$$\left(\begin{array}{ccccccc} 1 & 1 & 1 & 0 & 0 & 0 & 0 \\ 0 & 0 & 0 & 1 & 1 & 0 & 0 \\ 0 & 0 & 0 & 0 & 0 & 1 & 1 \\ -1 & 0 & 0 & -1 & 0 & -1 & 0 \\ 0 & -1 & 0 & 0 & 0 & 0 & 0 \\ 0 & 0 & -1 & 0 & -1 & 0 & -1 \end{array} \right) \cdot \left(\begin{array}{c} \psi_{14} \\ \psi_{16} \\ \psi_{16} \\ \psi_{24} \\ \psi_{26} \\ \psi_{34} \\ \psi_{36} \end{array} \right) \;=\; \left(\begin{array}{c} \Phi_1 \\ \Phi_2 \\ \Phi_3 \\ \Phi_4 \\ \Phi_5 \\ \Phi_6 \end{array} \right) \quad . \tag{11}$$

If the matrix A has rank $N_{\mathcal{D}}$ then the algebraic relationship (9) can be inverted and the apportionment of domain fluxes ψ_{ij} is determined uniquely from the source fluxes alone. It is well known in graph theory that the rank of an incidence matrix is one fewer than its number of vertices [19];

$$\mathrm{rank}(\mathrm{A}) = N_S - 1 \quad , \tag{12}$$

for a domain graph. Thus unique apportionment occurs only when $N_{\mathcal{D}} = N_S - 1$.

A graph with one fewer edge than vertices is called a *tree*, and is characterized by having one and only one path connecting any pair of vertices. (Figure 2a is an example of a tree.) If the domain graph is a tree then relationship (9) is solved by locating a "leaf" on the tree, which is a source i connected to only one domain $\mathcal{D}_{ij}$ (every tree must have leaves). It is trivial to solve this row of the flux relationship $\psi_{ij} = |\Phi_i|$. The corresponding row and column may be algebraically eliminated from (9) and the vertex and edge removed from the graph. The new graph still has one fewer edges than vertices and thus is still a tree. The process may be repeated solving for the next leaf and so on until all domain fluxes have been found. The final equation is mathematically over-specified since it contains two sources coupled to a single domain. Since the sum of all source fluxes was zero to begin with, both of the remaining fluxes will have the same magnitude, and the domain flux may be determined from either one.

2.2 Domain circuits and isolating loops

If the domain graph has more than $N_S - 1$ edges it is not a tree, the incidence matrix is rank deficient, and relation (9) cannot be inverted. Because the graph is not a tree, it contains at least one *circuit* of edges. We define an $N_{\mathcal{D}}$-element circuit vector $\vec{\mathcal{C}}$ by tracing the circuit in one direction and setting to $+1$ the elements denoting domains traversed in the forward direction (from positive to negative) and -1 for domains traversed in the reverse direction. Two circuits in figure 2b are labeled C_1 and C_2. Following C_1 in the clockwise sense its circuit-vector is

$$\begin{array}{ccccccccccc} & & & \mathcal{D}_{14} & \mathcal{D}_{15} & \mathcal{D}_{16} & \mathcal{D}_{24} & \mathcal{D}_{26} & \mathcal{D}_{34} & \mathcal{D}_{36} & \\ \vec{\mathcal{C}}_1 & = & [& 0 & 0 & 0 & +1 & -1 & -1 & +1 &] \end{array} ,$$

Choosing instead to traverse the circuit in the counter-clockwise sense, would simply change the sign of the circuit vector.

Since each vertex touched by the circuit will be encountered once in the forward and once in the reverse direction, it can be shown that

$$\mathrm{A} \cdot \vec{\mathcal{C}} = 0 \quad . \tag{13}$$

A circuit is therefore in the null-space of the incidence matrix. In physical terms, a circuit vector defines a flux re-apportionment between certain domains

$$\vec{\psi} \to \vec{\psi} + \delta\psi\, \vec{\mathcal{C}} \quad , \tag{14}$$

which can be performed without changing the flux relation (9). This re-apportionment is the topological manifestation of magnetic reconnection: field lines with certain foot-point connection (domains with negative entries in $\vec{\mathcal{C}}$) are transformed into field lines with different footpoint connections. If the effected domains come into spatial contact this foot-point re-assignment may be envisioned as the breaking and re-attaching of field lines at some location where the domains meet.

From another mathematical theorem we find that our graph contains exactly $N_{\mathcal{S}} - N_{\mathcal{D}} + 1$ "independent" circuits [19]. To see this consider breaking a circuit by removing from the graph any one of its edges, called a chord. Circuit C_1 in fig. 2b is broken by removing domain $\mathcal{D}_{34}$ as shown in fig. 3a. The graph will remain connected since there is an alternate pathway connecting the pair of vertices (3 and 4) previously connected by the chord. The new graph will have the same number of vertices and one fewer edge. If it still has more than $N_{\mathcal{S}} - 1$ edges, then it is not yet a tree and at least one circuit remains. The next circuit found will be independent of the first in the sense that it survived when the first circuit was broken. This process can be continued by removing edges until only $N_{\mathcal{S}} - 1$ remain, and the graph is a tree. In this demonstration a total of $N_c \equiv N_{\mathcal{D}} - N_{\mathcal{S}} + 1$ independent circuits, denoted $\mathcal{C}_\sigma$, are found (they were "broken" only as a means to count them). The N_c circuit vectors $\vec{\mathcal{C}}_\sigma$ will be linearly independent since each contains a non-zero entry at its chord, where all subsequent vectors will have zeros. The corresponding circuit vectors therefore span the entire N_c-dimensional null-space of the matrix A.

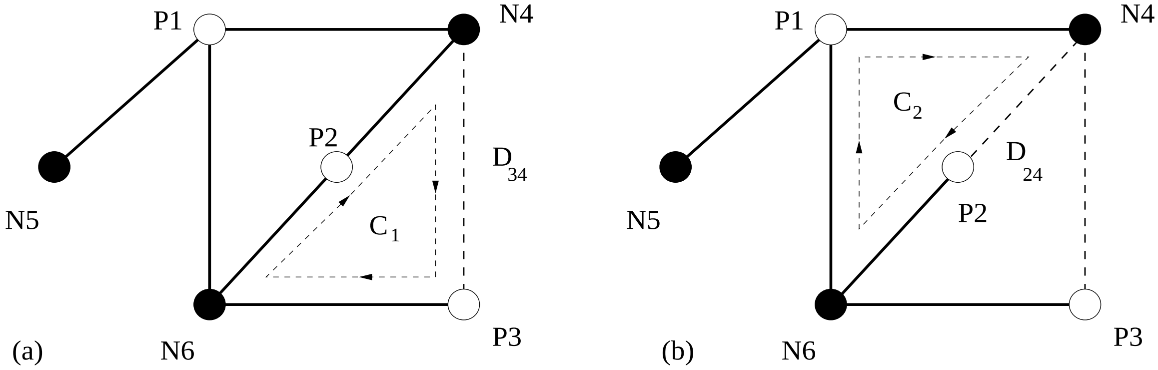

Figure 3. The process of identifying fundamental circuits in a graph. (a) One circuit, C_1, is located and broken by removing one of its edges, $\mathcal{D}_{34}$ (dashed), called a chord. (b) A second circuit, C_2, is found and broken by removing the edge $\mathcal{D}_{24}$. After this the graph is a tree with 6 vertices and 5 edges.

For each circuit $\mathcal{C}_\sigma$ we define a closed space-curve $\mathcal{Q}_\sigma$ in the corona, called its *isolating loop*. The space-curve follows the interfaces between domains, i.e. *separatrices*, and links C_σ exactly once. This definition of an isolating loop leaves considerable freedom in its exact spatial location. The "loop" is, in fact, a surface consisting of all its continuous deformations; we elaborate on this below.

Since it lies on separatrices, domains pass through $\mathcal{Q}_\sigma$ in their entirety either forward or backward. The loop-vector $\vec{\mathcal{Q}}_\sigma$ is defined with elements $+1$ or -1 for domains passing through in the forward or reverse sense. Because it links $\mathcal{C}_\sigma$ exactly once

$$\vec{\mathcal{C}}_\sigma \cdot \vec{\mathcal{Q}}_\sigma = 1 \quad . \tag{15}$$

The total flux through isolating loop $\mathcal{Q}_\sigma$, denoted Ψ_σ, is the sum of the fluxes of all domains

$$\Psi_\sigma = \oint_{\mathcal{Q}_\sigma} \mathbf{A} \cdot d\mathbf{l} = \vec{\mathcal{Q}}_\sigma \cdot \vec{\psi} \quad . \tag{16}$$

One choice for an isolating loop is a curve encircling the chord domain $\mathcal{D}_{ij}$ from the circuit $\mathcal{C}_\sigma$. The loop-vector would have a single non-zero element corresponding to the chord domain. The non-zero element would be either $+1$ or -1 depending on the sign of the corresponding element in $\vec{\mathcal{C}}_\sigma$ as required by (15). If we remove a particular sequence of chords to reduce the graph to a tree, then a given chord will appear in no subsequent circuits. This fact demonstrates that the loop-vectors so constructed will be linearly independent of one another.

Figure 4 shows an example of an isolating loop $\mathcal{Q}_1$ linking circuit $\mathcal{C}_1$ exactly once. The loop encircles only the domain $\mathcal{D}_{34}$ and will correspond to the vector

$$\begin{array}{cc} & \begin{array}{ccccccc} \mathcal{D}_{14} & \mathcal{D}_{15} & \mathcal{D}_{16} & \mathcal{D}_{24} & \mathcal{D}_{26} & \mathcal{D}_{34} & \mathcal{D}_{36} \end{array} \\ \vec{\mathcal{Q}}_1 = & \left[\begin{array}{ccccccc} 0 & 0 & 0 & 0 & 0 & -1 & 0 \end{array} \right] \end{array} ,$$

There are other choices for a given $\mathcal{Q}_\sigma$ and we will not require that each enclose a single domain; we will require that the loop-vectors be linearly independent.

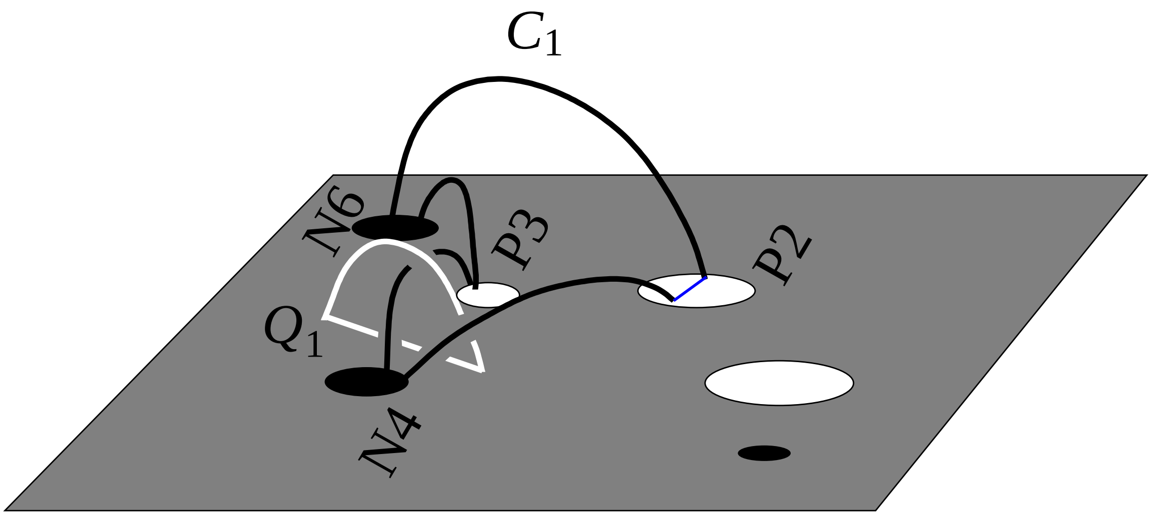

Figure 4. The physical location of circuit $\mathcal{C}_1$ (back solid line) along with an isolating loop $\mathcal{Q}_1$ (white solid line) which links it exactly once. The loop shown encircles the chord $\mathcal{D}_{34}$ of the circuit, and no other domains.

Adding all loop fluxes to the column vector $\vec{\Phi}$, and all loop-vectors $\vec{\mathcal{Q}}_\sigma$ as additional rows in A, leads to an expanded flux relation

$$\left[\begin{array}{c} \mathrm{A} \\ \\ \hline \vec{\mathcal{Q}}_1 \\ \vdots \\ \vec{\mathcal{Q}}_{N_c} \end{array}\right] \cdot \vec{\psi} \;=\; \left[\begin{array}{c} \vec{\Phi} \\ \\ \hline \Psi_1 \\ \vdots \\ \Psi_{N_c} \end{array}\right] \tag{17}$$

The loop-vectors are linearly independent and compliment the null space of A, so the relation above is of full rank and may be inverted. The domain fluxes are completely determined by the source fluxes along with the N_c loop fluxes. Our example is represented by the 7×8 system

$$\left(\begin{array}{ccccccc} 1 & 1 & 1 & 0 & 0 & 0 & 0 \\ 0 & 0 & 0 & 1 & 1 & 0 & 0 \\ 0 & 0 & 0 & 0 & 0 & 1 & 1 \\ -1 & 0 & 0 & -1 & 0 & -1 & 0 \\ 0 & -1 & 0 & 0 & 0 & 0 & 0 \\ 0 & 0 & -1 & 0 & -1 & 0 & -1 \\ \hline 0 & 0 & 0 & 0 & 0 & -1 & 0 \\ 0 & 0 & 0 & -1 & 0 & 0 & 0 \end{array}\right) \cdot \left(\begin{array}{c} \psi_{14} \\ \psi_{16} \\ \psi_{16} \\ \psi_{24} \\ \psi_{26} \\ \psi_{34} \\ \psi_{36} \end{array}\right) = \left(\begin{array}{c} \Phi_1 \\ \Phi_2 \\ \Phi_3 \\ \Phi_4 \\ \Phi_5 \\ \Phi_6 \\ \hline \Psi_1 \\ \Psi_2 \end{array}\right) \quad , \tag{18}$$

where the horizontal bars separate the additional loops and additional isolating-fluxes.

In addition to the boundary conditions it is necessary to constrain N_c fluxes Ψ_1, $\Psi_2, \ldots,$ Ψ_{N_c} in order to fix all $N_\mathcal{D}$ domain fluxes. From all fields satisfying these N_c constraints, there will be one whose magnetic energy is the minimum; this is the stable equilibrium. For a set of boundary conditions $f(x, y)$ and connections $\mathcal{G}$ there will be an N_c-dimensional space of such minimum-energy equilibria.

3 The minimum-energy field

The magnetic field whose energy is a minimum, subject boundary condition (1), may be found using the calculus of variations. To assure a solenoidal solution we vary the vector potential $\mathbf{A}(\mathbf{x})$ subject to boundary conditions on its tangential components. Equation (2) gives the magnetic energy functional for a volume $\mathcal{V}$, the half-space $z > 0$. The variation is performed by adding a small perturbation to the vector potential, $\mathbf{A} \to \mathbf{A} + \delta\mathbf{A}$, and expanding the integral to first order

$$\delta W \;=\; \int\limits_{\mathcal{V}} \mathbf{B} \cdot \nabla \times \delta\mathbf{A}\, d\mathbf{x} \;=\; \oint\limits_{\partial\mathcal{V}} \delta\mathbf{A} \times \mathbf{B} \cdot \hat{\mathbf{n}}\, dS \;+\; \int\limits_{\mathcal{V}} \nabla \times \mathbf{B} \cdot \delta\mathbf{A}\, d\mathbf{x} \quad . \tag{19}$$

The surface integral on the right hand side is always zero, since $\hat{\mathbf{n}} \times \delta\mathbf{A} = 0$ at each point on $\partial\mathcal{V}$. In order that $\delta W = 0$ under arbitrary variation, $\delta\mathbf{A}$, we must have $\nabla \times \mathbf{B} = 0$ everywhere inside $\mathcal{V}$. Thus follows the well-known result that a potential field, also called a vacuum field, is the state of minimum magnetic energy.

It is also possible to perform the variational calculation subject to constraints on a set of domain fluxes ψ_{ij}. The structure of the constraints is summarized by a graph $\mathcal{G}_c$ and quantified by the vector of domain fluxes $\vec{\psi}_c$. The vacuum field, which satisfies the unconstrained problem, will have a domain graph $\mathcal{G}_v$ whose fluxes are a vector $\vec{\psi}^{(\mathrm{v})}$. If the constraint graph and the vacuum graph are different, then the problem must be reposed as one with the larger graph $\mathcal{G} = \mathcal{G}_c \cup \mathcal{G}_v$ and domain fluxes $\psi_{ij} = 0$ for each domain not present in $\mathcal{G}_c$. Henceforth we will assume that the constraint graph $\mathcal{G}$ is so constructed and therefore includes $\mathcal{G}_v$ as a subgraph.

If the constraint graph is a tree, and the vacuum graph is connected, then $\mathcal{G}_v$ must be the same tree. In this case the domain fluxes $\vec{\psi}$ are uniquely determined by the source fluxes $\vec{\Phi}$. The vacuum field will therefore automatically satisfy the constraints and will be the minimum energy state of the constrained system.

The only alternative is that the constraint graph $\mathcal{G}$ contains one or more circuits and is therefore not a tree. In this case the domain fluxes in the vacuum field, $\vec{\psi}^{(\mathrm{v})}$, will in general differ from the constraints $\vec{\psi}_c$. In order to find the minimum energy field from those with prescribed domain fluxes we must perform a constrained variation. In a graph with $N_{\mathcal{D}}$ domains and N_S sources, it is sufficient to constrain the fluxes through $N_c = N_{\mathcal{D}} - N_S + 1$ independent isolating loops in order to constrain all domain fluxes. Each constraint is applied using a constraint functional

$$G_\sigma\{\mathbf{A}(\mathbf{x})\} \;=\; \oint_{\mathcal{Q}_\sigma} \mathbf{A}\cdot d\mathbf{l} - \Psi_\sigma \;=\; 0 \quad , \tag{20}$$

which vanishes so long as the constraint on $\mathcal{Q}_\sigma$ is satisfied.

The isolating loop $\mathcal{Q}_\sigma$ is defined to pass along separatrices and link circuit $\mathcal{C}_\sigma$ of the domain graph $\mathcal{G}$. There are, in general, a family of topologically equivalent space-curves satisfying this definition, and the flux through every one must be the same. This family of loops forms a two dimensional surface to be called the *isolating sheet* $\mathcal{S}_\sigma$. By its construction the isolating sheet is topologically annular and is constructed from pieces of one or more separatrices.

The isolating sheet $\mathcal{S}_\sigma$ can be written as the parameterized surface $\mathbf{x}_\sigma(\xi,\eta)$ where the coordinate $\eta \in [0,1]$ labels particular isolating loops and $\xi \in [0,1]$ follows along the loop. Coordinates $\xi = 0$ and $\xi = 1$ are identified for each loop (see fig. 5) since each one is by definition closed. In general an isolating sheet may consist of several distinct annular surfaces, called folds, each of which will have the simple structure depicted in fig. 5. The foregoing argument may be easily generalized to include multiple folds, but for simplicity we consider one fold per sheet. The constraint functional

$$G_\sigma\{\mathbf{A}(\mathbf{x})\} \;=\; \int \lambda_\sigma(\eta)\left[\oint \frac{\partial \mathbf{x}_\sigma}{\partial \xi}\cdot \mathbf{A}(\mathbf{x})\,d\xi \;-\; \Psi_\sigma\right] d\eta$$

$$= \int \lambda_\sigma(\eta) \left[\frac{\partial \mathbf{x}_\sigma}{\partial \xi} \cdot \mathbf{A}(\mathbf{x}) \ - \ \Psi_\sigma \right] |\nabla\xi \times \nabla\eta| \, \delta(\mathcal{S}_\sigma) \, d\mathbf{x} \ = \ 0 \quad , \tag{21}$$

includes an integral over loops η, with a different undetermined multiplier on each one. The second expression is a volume integral using a one-dimensional delta-function $\delta(\mathcal{S}_\sigma)$ confined to the sheet $\mathcal{S}_\sigma$.

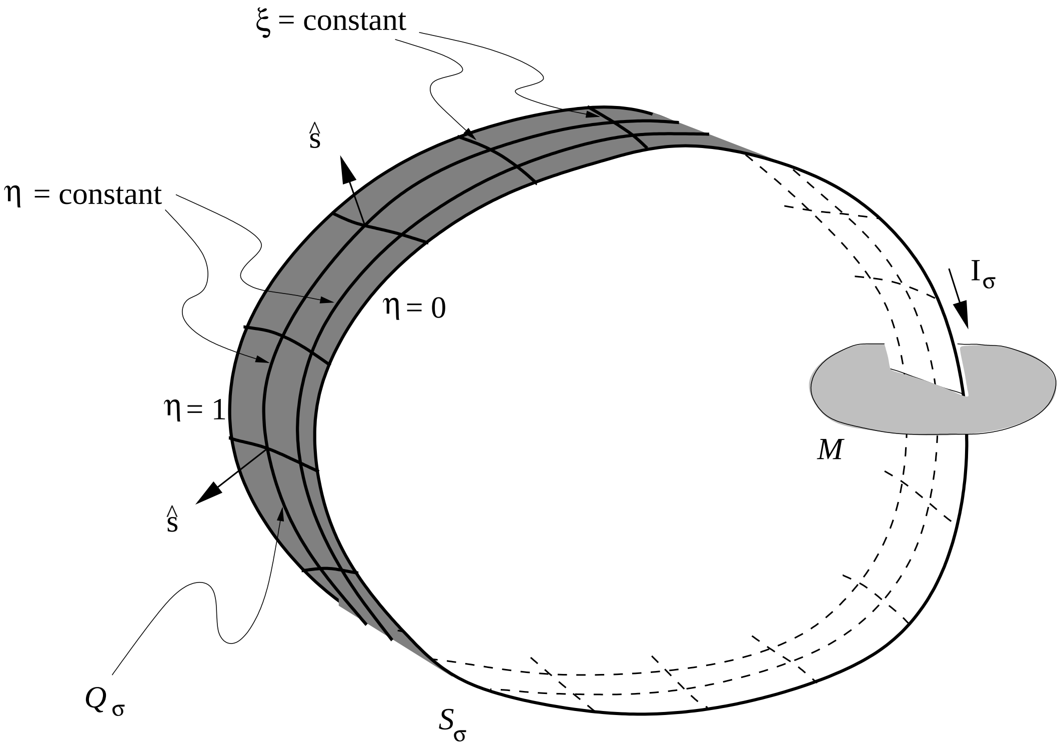

Figure 5. A schematic of the isolating sheet $\mathcal{S}_\sigma$ composed of continuous deformations of a single isolating loop $\mathcal{Q}_\sigma$. The surface is parameterized by coordinates (ξ, η). The edges of the surface are $\eta = 0$ and $\eta = 1$.

In addition to the flux constraint, it is necessary that each isolating sheet $\mathcal{S}_\sigma$ remain on a separatrix surface even under variations of $\mathbf{A}(\mathbf{x})$. That is to say, the normal component of $\nabla \times \mathbf{A}$ must vanish at each point of $\mathcal{S}_\sigma$. This requirement is enforced by a second set of functionals

$$H_\sigma\{\mathbf{A}(\mathbf{x})\} = \int \mu_\sigma(\xi, \eta) \, \hat{\mathbf{s}} \cdot (\nabla \times \mathbf{A}) \, \delta(\mathcal{S}_\sigma) \, d\mathbf{x} \ = \ 0 \quad , \tag{22}$$

where $\hat{\mathbf{s}}$ is the normal to $\mathcal{S}_\sigma$, and μ_σ is a function of both coordinates in order to enforce the point-wise constraint.

Subtracting all $2N_c$ constraint functionals from the energy (2) and performing a variation over the vector potential $\mathbf{A}(\mathbf{x})$, while holding fixed the isolating sheets, yields the Euler-Lagrange equation

$$\nabla\times\mathbf{B} \;=\; \sum_{\sigma=1}^{N_c}\left\{\lambda_\sigma(\eta)\,|\nabla\xi\times\nabla\eta|\frac{\partial\mathbf{x}_\sigma}{\partial\xi} \;+\; \nabla\mu_\sigma\times\hat{\mathbf{s}}\right\}\delta(\mathcal{S}_\sigma) \;=\; \sum_\sigma \mathbf{J}_\sigma(\mathbf{x}) \quad . \tag{23}$$

The current density on the right hand side consists of a number of surface currents confined to the isolating sheets $\mathcal{S}_\sigma$. The field is current-free within the entire volume of each coronal domain.

The total current on a particular sheet must pass through a membrane $\mathcal{M}$ punctured by it (see fig. 5)

$$\begin{aligned} I_\sigma \;&=\; \oint_{\partial\mathcal{M}}\mathbf{B}\cdot d\mathbf{l} \;=\; \int_{\mathcal{M}\cap\mathcal{S}_\sigma}\left\{\lambda_\sigma\,|\nabla\xi\times\nabla\eta|\frac{\partial\mathbf{x}_\sigma}{\partial\xi} \;+\; \nabla\mu_\sigma\times\hat{\mathbf{s}}\right\}\cdot\hat{\mathbf{s}}\times d\mathbf{l} \\ &=\; \int_0^1\lambda_\sigma(\eta)\,d\eta \;+\; \int_{\mathcal{M}\cap\mathcal{S}_\sigma}\nabla\mu_\sigma\cdot d\mathbf{l} \end{aligned} \tag{24}$$

In order that the Euler-Lagrange equation be solvable, I_σ must be constant along the loop. For this to be so the integral of $\nabla\mu_\sigma$ between the edges must be independent of $\mathcal{M}$. This in turn requires μ_σ to be constant along along each edge of the sheet (referring to [23] this is equivalent to demanding no surface current normal to the edge). It is always possible to redefine $\lambda_\sigma(\eta)$ and $\mu_\sigma(\xi,\eta)$ so that $\mu_\sigma(\xi,0)=\mu_\sigma(\xi,1)=0$, and the integral of $\lambda_\sigma(\eta)$ is the total current I_σ. We will henceforth assume this definition of λ and μ.

The combined functional must also vanish under independent variations in the location of each sheet $\mathbf{x}_\sigma(\xi,\eta)\to\mathbf{x}_\sigma(\xi,\eta)+\delta\mathbf{x}_\sigma(\xi,\eta)$. Since the energy functional W is an integral over $\mathcal{V}$ its value will not change under this variation. Stationarity under variations must, however, be demanded from the pair of constraint functionals

$$G_\sigma + H_\sigma \;=\; \int\left[\lambda_\sigma(\eta)\,\mathbf{A}\cdot\frac{\partial\mathbf{x}_\sigma}{\partial\xi} \;+\; \mu(\xi,\eta)\,\mathbf{B}\cdot\frac{\partial\mathbf{x}_\sigma}{\partial\xi}\times\frac{\partial\mathbf{x}_\sigma}{\partial\eta}\right]d\xi\,d\eta \;-\; I_\sigma\Phi_\sigma \quad , \tag{25}$$

which clearly depend on the location of the sheet. Introducing the perturbations and integrating by parts over ξ or η, yields the expression

$$\delta G_\sigma + \delta H_\sigma \;=\; \int\left[\lambda_\sigma\frac{\partial\mathbf{x}_\sigma}{\partial\xi} \;+\; \nabla\mu\times\left(\frac{\partial\mathbf{x}_\sigma}{\partial\xi}\times\frac{\partial\mathbf{x}_\sigma}{\partial\eta}\right)\right]\times\mathbf{B}\cdot\delta\mathbf{x}_\sigma\;d\xi\,d\eta \quad , \tag{26}$$

where boundary terms in ξ vanish since it is periodic, and in η vanish since $\mu_\sigma=0$ at the sheet edges $\eta=0$ and $\eta=1$. Converting this to a volume integral gives

$$\delta G_\sigma + \delta H_\sigma \;=\; \int_{\mathcal{V}}(\mathbf{J}_\sigma\times\mathbf{B}\cdot\delta\mathbf{x}_\sigma)\,d\mathbf{x} \;=\; 0 \quad , \tag{27}$$

where $\mathbf{J}_\sigma$ is the current density from the right hand side of expression (23). This volume integral must vanish for arbitrary perturbations $\delta\mathbf{x}_\sigma(\xi,\eta)$ to the sheet $\mathcal{S}_\sigma$.

This is equivalent to requiring *weak* force balance of the current in the sheet, namely magnetic pressure balance across the sheet [20].

Any solution to (23) and (27) will make the energy stationary under all variations. This is an extremum of the energy, but not necessarily a minimum. The energies of all admissible fields are bounded from below by the vacuum field energy, thus we expect at least one minimum-energy field within those satisfying the flux constraints. This minimum will necessarily satisfy (23) and (27) subject to boundary conditions (1) and flux constraints. There may be other solutions which are saddle-type extrema (it is unlikely that there is a state with maximum magnetic energy), but we henceforth consider only the minimum energy solution, characterized by the N_c fluxes Ψ_σ and N_c currents I_σ.

3.1 Free energy

The minimizing magnetic field may be decomposed into a potential field satisfying the boundary condition (1) and a homogeneous-nonpotential field satisfying (23) with vanishing normal components on $\partial\mathcal{V}$. The total magnetic energy is the sum of the potential and homogeneous-nonpotential pieces separately

$$W \;=\; \frac{1}{2}\int_{\mathcal{V}} |\mathbf{B}^{(\mathrm{v})}|^2\, d\mathbf{x} \;+\; \frac{1}{2}\int_{\mathcal{V}} |\mathbf{B}^{(\mathrm{np})}|^2\, d\mathbf{x} \quad , \tag{28}$$

since the cross term vanishes (to see this, write $\mathbf{B}^{(\mathrm{v})} = -\nabla\chi$ and integrate the term by parts). The non-potential field arises due to the constraints placed on flux domains, so its energy

$$\Delta W \;=\; \frac{1}{2}\int_{\mathcal{V}} |\mathbf{B}^{(\mathrm{np})}|^2\, d\mathbf{x} \;=\; \frac{1}{2}\int_{\mathcal{V}} \mathbf{J}\cdot\mathbf{A}^{(\mathrm{np})}\, d\mathbf{x} \quad , \tag{29}$$

can be considered the topological energy [21] associated with flux constraints.

The variational procedure showed that the current density $\mathbf{J}$ is confined to topologically annular sheets $\mathcal{S}_\sigma$ carrying current I_σ. This fact may be used to re-write the non-potential energy as

$$\Delta W \;=\; \frac{1}{2}\sum_\sigma I_\sigma\, \bar{\Psi}_\sigma^{(\mathrm{np})} \quad , \tag{30}$$

where $\bar{\Psi}_\sigma^{(\mathrm{np})}$ is the flux from $\mathbf{B}^{(\mathrm{np})}$ averaged over the current paths in $\mathcal{S}_\sigma$. Since it lies on a separatrix, field lines from the total magnetic field $\mathbf{B}^{(\mathrm{v})} + \mathbf{B}^{(\mathrm{np})}$ do not cross $\mathcal{S}_\sigma$; each field separately will, however, have a non-vanishing component normal to $\mathcal{S}_\sigma$.

A separate energy calculation uses a continuous transition to the equivalently connected potential magnetic field $\mathbf{B}^{(\mathrm{v})}(\mathbf{x})$. Supplementing its domain graph $\mathcal{G}_v$ with domains of zero flux in order to make it equivalent to $\mathcal{G}$, each isolating sheet in $\mathbf{B}$, corresponds to one in $\mathbf{B}^{(\mathrm{v})}$. The fluxes enclosed by these loops are Ψ_σ and $\Psi_\sigma^{(\mathrm{v})}$ respectively. If

$$\Delta\Psi_\sigma \;\equiv\; \Psi_\sigma - \Psi_\sigma^{(\mathrm{v})} \quad , \tag{31}$$

were zero for each isolating loop, then the flux constraints would be satisfied by a potential magnetic field; this would clearly be the minimum-energy field.

The free energy of a general field may be calculated by summing the energies required to change the potential fluxes $\Psi_\sigma^{(\mathrm{v})} \to \Psi_\sigma$ one at a time. Changing the flux Ψ_ρ, requires an energy

$$\Delta W_\rho \;=\; -\int dt \left[\int \sum_\sigma \mathbf{J}_\sigma \cdot \mathbf{E}\, d^3\mathbf{x}\right] \;=\; \int_{\Psi_\rho^{(\mathrm{v})}}^{\Psi_\rho} I_\rho(\Psi_\sigma)\, d\Psi_\rho \quad , \tag{32}$$

since fluxes in all other loops $\mathcal{Q}_\sigma$ are fixed during this change. In this expression the current I_ρ is defined to be positive in the direction producing a self-flux oriented as $\Psi_\rho^{(\mathrm{v})}$ (i.e. using the right-hand rule). The total free energy is found by adding the contributions from changing each flux in turn. Since the final magnetic field is independent of the order in which the fluxes are changed, the energy will depend only on the set of flux differences $\Delta W(\Delta\Psi_\sigma)$. The minimum of this function will be $\Delta W(\mathbf{0}) = 0$ corresponding to domain fluxes consistent with a potential magnetic field.

For small, continuous departures from a potential field, i.e. small currents I_σ, the isolating loops in $\mathbf{B}$ will be spatially close to those in $\mathbf{B}^{(\mathrm{v})}$. Averaging the *potential* flux over the current-paths in a sheet will yield an answer similar to $\Psi^{(\mathrm{v})}$, and

$$\bar{\Psi}_\sigma^{(\mathrm{np})} \;=\; \Psi_\sigma \;-\; \bar{\Psi}_\sigma^{(\mathrm{v})} \;\simeq\; \Delta\Psi_\sigma \quad . \tag{33}$$

Replacing this in (30) gives an expression for the energy for small $\Delta\Psi_\sigma$

$$\Delta W \;\simeq\; \tfrac{1}{2}\sum_\sigma I_\sigma(\Delta\Psi_\rho)\,\Delta\Psi_\sigma \quad , \tag{34}$$

where each current I_σ will depend on the fluxes loops other than its own. In order that ΔW be minimum at a potential field it is necessary that $I_\sigma(\mathbf{0}) = 0$. The minimum current corona (MCC) is quantified in this small-current limit [14].

4 An example in two dimensions

4.1 The geometry

It is illuminating to apply the above procedure to the well-studied case of a two-dimensional, quadrupolar magnetic field [10, 22]. Assuming boundary sources which are translationally symmetric in x immediately means $B_x = 0$ in the minimum energy state, since line-tying is not present to maintain a magnetic shear. For simplicity we restrict the calculation to a finite portion of the system, extending from $x = 0$ to $x = L$, by placing conducting boundaries at these two planes. Four flux sources are strips of alternating polarity on the $z = 0$ plane (see fig. 6). The sources will be interconnected in all four possible ways, leading to a square domain graph which is itself the only circuit, $\mathcal{C}_1$. The isolating loop $\mathcal{Q}_1$, shown in fig. 6, encloses only domain $\mathcal{D}_{23}$. It follows any of the separatrices from $x = 0$ to $x = L$, follows the $x = L$ end-plane down to a point between $N2$ and $P3$ on the $z = 0$ plane, follows the photosphere back to the $x = 0$ end-plane and then proceeds up that end-plane to close.

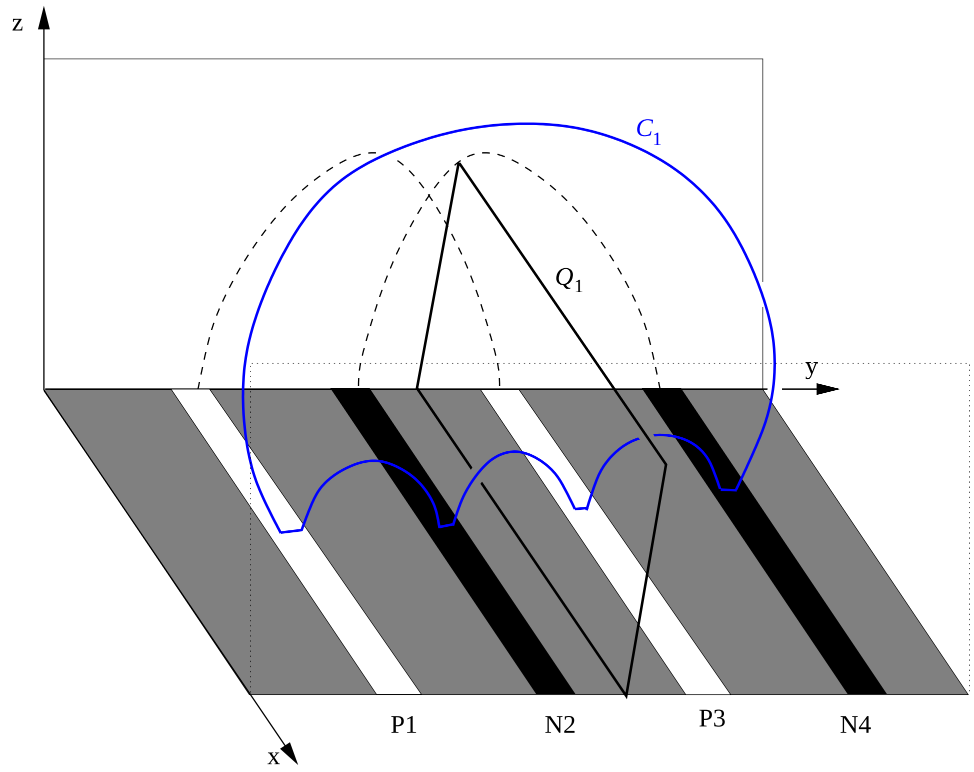

Figure 6. The geometry of the two-dimensional magnetic field. End-planes at $x = 0$ and $x = L$ confine the field. Strips of boundary flux $P1$, $N2$, $P3$ and $N4$ are the four sources. Field lines from the circuit $\mathcal{C}_1$ are grey, and the isolating loop $\mathcal{Q}_1$ which links it once is shown in black.

Topologically, the circuit $\mathcal{C}_1$ is a square whose interior includes all four domains. The separatrices must intersect any membrane bounded by $\mathcal{C}_1$. In special cases (e.g a potential field) all four boundaries will meet at a single line, as shown in fig. 7a. More generically the domains meet three at a time along two distinct lines, as shown in fig. 7b and 7c. In the generic case the isolating sheet, $\mathcal{S}_1$, consists of five folds: two A-type separatrices terminating in positive sources, two B-type separatrices, terminating in negative sources, and one surface R with Y-points at each end.

The field which minimizes the constrained energy functional will be current-free in all four domains, and will contain surface currents confined to the isolating sheet described above. To be in force balance $|\mathbf{B}|$ must be continuous across a current sheet. In two dimensions this means that $\mathbf{B}$ must reverse direction across the sheet. Such a

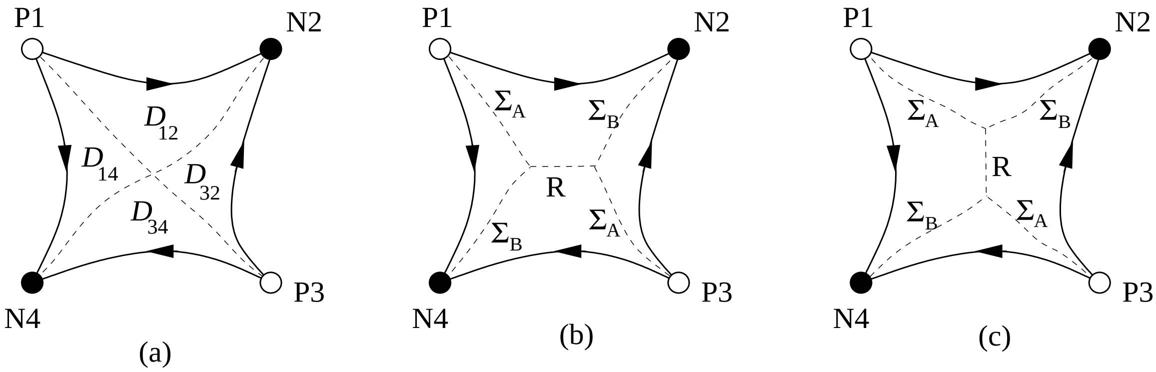

Figure 7. The three possible configurations for the separatrices. Configuration (a) is a special case, while (b) and (c) are two generic possibilities.

reversal is impossible on separatrices Σ_A or Σ_B since they terminate at sources where the field is unidirectional. We are thus forced to the conclusion that the surface R is the only fold of the isolating sheet which admits current.

The orientation of the current sheet, and the sense of current within it, are determined by the flux constraint Ψ_1. In the case depicted in fig. 7b, domains $\mathcal{D}_{12}$ and $\mathcal{D}_{34}$ meet at surface R. These domains have rightward and leftward fields respectively, causing current in $\mathcal{S}_1$ to flow in the $-\hat{\mathbf{x}}$ direction (into the page). This sense of current creates an average non-potential flux leftward through through the isolating loop, in the same sense as the field in $\mathcal{D}_{23}$. This then corresponds to a case where $\Psi_1 > \Psi_1^{(\mathrm{v})}$ the flux in the vacuum field.

Conversely, the case with $\Psi_1 < \Psi^{(\mathrm{v})}$ will correspond to the configuration from 7c. An equilibrium field of this type is shown in 8b. The potential field arising from the same boundary conditions, shown in 8a, has $\Psi_1^{(\mathrm{v})} = 0.4\Phi_3$. The non-potential field contains a vertical sheet with current in the $+\hat{\mathbf{x}}$ direction, and has $\Psi_1 = 0.3\Phi_3 < \Psi_1^{(\mathrm{v})}$. Figure 8c shows the field lines of the homogeneous nonpotential part of the field.

4.2 An analytic treatment

The magnetic field can be written using the vector potential $\mathbf{A} = A(y,z)\hat{\mathbf{x}}$, where $A(y,z)$ will be harmonic in all domains, and thus may be written as the real part of a complex function of the complex coordinate $w = y + iz$ [11]. The homogeneous-nonpotential piece of this function is given by an integral

$$A^{(\mathrm{np})}(w) \;=\; \frac{1}{2\pi}\mathrm{Re}\int_0^1 \lambda(\eta)\,\ln\left[\frac{w-\zeta^*(\eta)}{w-\zeta(\eta)}\right]\,d\eta \;\;, \tag{35}$$

where the current sheet is located at $w = \zeta(\eta)$, and an image sheet below the photosphere, $w = \zeta^*(\eta)$, satisfies the homogeneous boundary condition $A(y,0) = 0$. The complex function is analytic everywhere except for a branch cut along the current

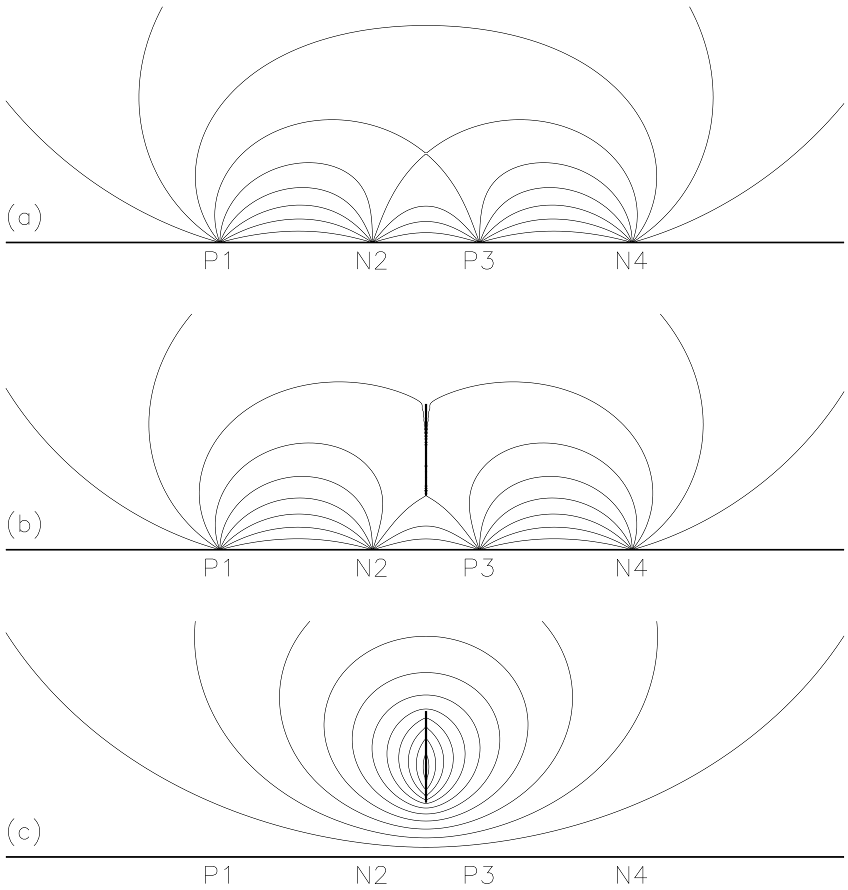

Figure 8. Equilibrium magnetic field lines corresponding to four magnetic sources. (a) The potential field, and (b) a non-potential field with $\Psi_1 < \Psi_1^{(\mathrm{v})}$. (c) The homogeneous-nonpotential field $\mathbf{B}^{(\mathrm{np})}$.

sheet $w = \zeta$. The vector potential is continuous along this branch cut (this is true of the real part of the complex logarithm) but its derivative is not.

The current sheet must be positioned so that it lies on a flux surface of the total magnetic field, and satisfies force balance. Both conditions are satisfied if the potential magnetic field at each point on the current sheet cancels the non-potential field averaged between the two sides of the sheet. This is equivalent to the Cauchy integral equation

$$B_z^{(\mathrm{v})}(w) + iB_y^{(\mathrm{v})}(w) \;=\; -\frac{1}{2\pi}\fint_R \lambda\left(\frac{d\zeta}{d\eta}\right)^{-1}\frac{\zeta-\zeta^*}{(w-\zeta)(w-\zeta^*)}\,d\zeta \quad , \tag{36}$$

at points $w = \zeta(\eta)$ on the current sheet (the principle value of the integral is used in this equation). This Cauchy integral transform can be inverted [23] along any curve $\zeta \in R$, provided R satisfies a solvability condition. Performing this inversion yields a unique complex function $\lambda/(d\zeta/d\eta)$, which does not, in general, correspond to a real current density $\lambda(\eta)$. The final step in finding the equilibrium field is to deform the complex curve R until the current density $\lambda(\eta)$ is real for all $\eta \in [0, 1]$.

In the vicinity of its X-point, $w = W_x$, the potential field may be expanded $B_z^{(\mathrm{v})} + iB_y^{(\mathrm{v})} = B'(w - W_x)$. If the sources are symmetric with respect to a reflection about $y = 0$ accompanying a change in their sign, then the current sheet will have the symmetry $\zeta^*(\eta) = -\zeta(1-\eta)$, the coefficient B' will be real, and $W_x = iZ_x$. Equation (36) can then be inverted for either a horizontal or vertical curve of length Δ centered on W_x (from the solvability condition), to give a real current density

$$\lambda(\eta) \;=\; \pm\, 2B'\Delta^2\sqrt{\eta(1-\eta)} \quad , \tag{37}$$

where the upper (lower) sign corresponds to a vertical (horizontal) current sheet. Expression (37) is the unique solution to (36) for which λ is bounded at $\eta = 0$ and $\eta = 1$; it is the Green-Syrovatskii current profile [8, 9]. The total current in the sheet is

$$I_1 \;=\; \pm\frac{\pi B'\Delta^2}{4} \quad . \tag{38}$$

Using (37) in the vector potential (35) and averaging over the currents gives an expression for the average nonpotential flux

$$\bar{\Psi}_1^{(\mathrm{np})} \;=\; \frac{I_1 L}{2\pi}\,\ln[8e^{1/2}Z_x/\Delta] \quad . \tag{39}$$

With a symmetric current sheet centered at the potential X-point, $\bar{\Psi}_1^{(\mathrm{v})} = \Psi_1^{(\mathrm{v})}$ and the factor in the energy $\bar{\Psi}_1^{(\mathrm{np})} = \Delta\Psi_1$. A concise relationship between current and flux change can be phrased in terms of the characteristic current for the potential X-point, $I_* \equiv B'Z_x^2$,

$$\Delta\Psi_1(I_1) \;=\; \frac{I_1 L}{4\pi}\,\ln[16\pi e\, I_*/|I_1|] \quad . \tag{40}$$

The current vanishes as $\Delta\Psi_1 \to 0$, as predicted in §3.1.

The analytic inversion of the Cauchy integral equation given above is valid in the vicinity of the X-point. This means that the expressions are strictly valid only in the limit $\Delta \ll Z_x$, or equivalently $|I_1| \ll I_*$. The equation can in principle be solved for all values of current up to the limiting cases where $\psi_{23} \to 0$, when $\mathcal{D}_{23}$ vanishes, and the limit $\psi_{23} \to \Psi_3 = |\Psi_2|$ where $\mathcal{D}_{12}$ and $\mathcal{D}_{34}$ both vanish. Both limiting cases involve topological changes, since the domain graph changes (in fact it becomes an unconnected graph), however, it is possible to approach the limits within the formalism developed above. Figure 9 shows the field for each limiting case. The limit $\psi_{23} \to 0$ contains a global vertical current sheet which evolved from the $\lambda > 0$ sheet such as that in fig. 8b. In the case $\psi_{23} = \Psi_3$ the $\lambda < 0$ horizontal current sheet has grown to completely surround $\mathcal{D}_{23}$. In neither of the limiting cases does the current sheet end in a Y-type point, as it does in all cases approaching the limit.

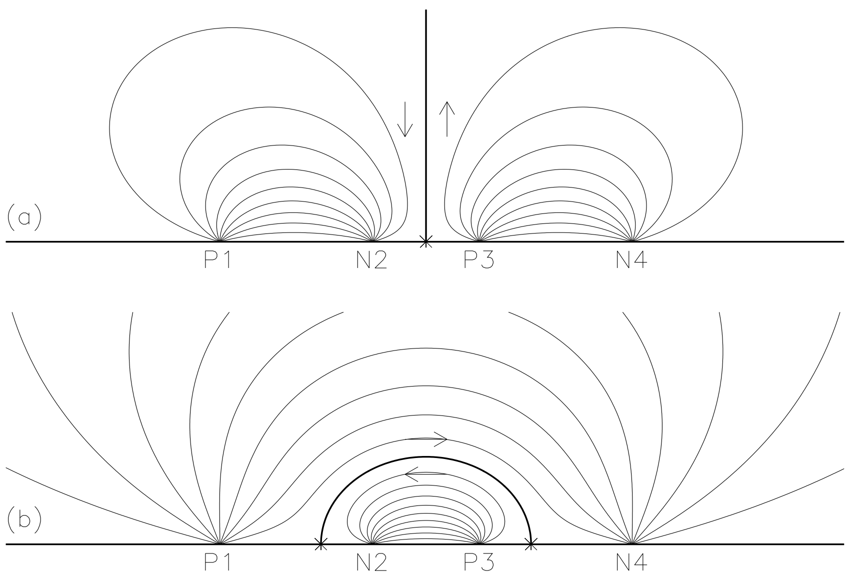

Figure 9. Limiting cases for the source distribution shown fig. 8). Contours of the vector potential $A(y, z)$ are plotted for (a) the case $\psi_{23} = 0$ and (b) the case $\psi_{23} = \Psi_3$. The current sheet is shown with a dark line, and the direction of field indicated by arrows. The null-points shown with $*$'s are of non-generic type arising in the limit of topological changes in the field.

The total current $I_1(\Psi_1)$ is a well behaved function over the entire range of domain flux $\Psi_1 = \psi_{23}$, achieving its maximum and minimum values in the limiting cases. In general the extreme values will be $|I_1| \sim I_*$, since that is the only characteristic current in the problem. For the example shown in fig. 9 the limiting currents are $+5.67\, I_*$ (9a) and $-9.46\, I_*$ (9b). Figure 10 shows the form of the current *vs* flux relationship. The analytic expression (40), shown dashed, comes surprisingly close to the limiting points, shown as asterisks, as well as to those cases which can be approximated numerically (such as fig. 8b).

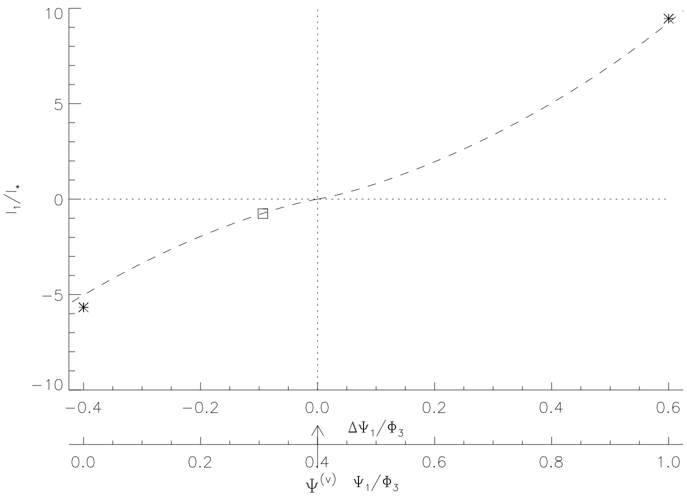

Figure 10. The current *vs* flux relationship for the source distribution from fig. 8. Current plotted is the $-\hat{\mathbf{x}}$ component to be consistent with the right-hand rule, normalized to I_*. The top abscissa is the non-potential flux $\Delta\Psi_1 = \Psi - \Psi_1^{(v)}$, while the bottom abscissa is the total flux Ψ_1; both are normalized to the source flux. The limiting cases fig. 9 are marked with $*$'s, and the vertical current sheet fig. 8b is shown with a square. The dashed curve is analytic expression (40).

4.3 General two-dimensional fields

This same analysis may be applied to two-dimensional magnetic fields of arbitrary complexity. In a general two-dimensional field, the domain graph must be planar and the domains form contiguous regions which fill the plane. An exhaustive treatment of all possible graphs is outside the scope of this work, but it is possible to make statements about the topologies of potential fields. Of course, properties of potential fields then apply to all equivalently connected fields. The potential $A(y, z)$ can be written as the real part of an analytic function, $F(w)$, as above. The derivative of the complex function will give the combination $B_z + iB_y = -F'(w)$. In the neighborhood of a generic null-point, W_x, the magnetic field will have a zero of first-order

$$B_z(w) + iB_y(w) \;\simeq\; B'(w - W_x) \quad , \tag{41}$$

where the coefficient B' may be complex. Zeros of higher order are not structurally stable, and will become clusters of first order nulls under arbitrarily small changes to the boundary condition.

In the neighborhood of the generic null-point W_x the potential has a saddle, representing a magnetic X-point

$$A(w) \ \simeq \ \mathrm{Re}[\,\tfrac{1}{2}B'(w-W_x)^2\,] \ + \ A_x \quad . \tag{42}$$

The four separatrix field lines connect to the null along lines where $\arg(w-W_x) = n\pi/2 - \arg(B')/2$, for $n = 0, 1, 2, 3$. Tracing each separatrix line from a coronal null ($\mathrm{Im}W_x > 0$), will, in general, lead to a photospheric source; cases where a separatrix line connects two magnetic nulls are not structurally stable.

If four different sources lie at the ends of the four separatrix lines then the domain graph contains a circuit connecting the four, equivalent to fig. 7a, The foregoing analysis of this circuit may be applied directly, reaching the conclusion that an isolating sheet must pass along the separatrices. In an equivalently connected field with current sheets, there will be one current sheet inside the circuit, in either of the orientations 7b or 7c. Thus, in an arbitrary two-dimensional field we expect current sheets at points related to X-points in the equivalently connected potential field. A general theory for this class of quasi-potential singular equilibria has been previously presented using harmonic functions of complex coordinates [11, 24].

5 Three-dimensional fields

A completely general treatment of three-dimensional fields follows from this same theory. It is simplest to study the topology for potential fields, since their properties have been carefully characterized [17, 14, 25]. This topology of the potential field can be applied to all equivalently connected non-potential fields.

Magnetic nulls in three-dimensions are classified as either A-type or B-type depending on their local geometry [26, 27]. The determinant of the Jacobian matrix $\partial B_i/\partial x_j$ will be positive at an A-type null and negative at a B-type null. There is a surface of field lines, the fan, entering an A-type and leaving a B-type null. Orthogonal to this surface are two field lines called spines, which leave/enter a null of A-type/B-type.

A separatrix surface between two domains must be composed of field lines, but these cannot terminate at the either of the sources which distinguish the domains (lest they actually belong to that domain, rather than the boundary). The separatrix must therefore originate (or terminate) at a magnetic null — it is the fan surface of that null. The separatrix between $\mathcal{D}_{ik}$ and $\mathcal{D}_{im}$ must map onto the positive photospheric source P_i (see fig. 11). This is a Σ_A separatrix which terminates at an A-type magnetic null somewhere. The spines of this null must map to negative sources N_k and N_m since they lie in domains $\mathcal{D}_{ik}$ and $\mathcal{D}_{im}$. Similarly, Σ_B separatrices, which map to negative source regions, are the fans of B-type nulls.

In a potential magnetic field, a Σ_A separatrix intersects a Σ_B along a single field line called a separator. This separator lies at the junction of four domains, as shown in fig. 11. The four domains surrounding a separator field line form a circuit in the

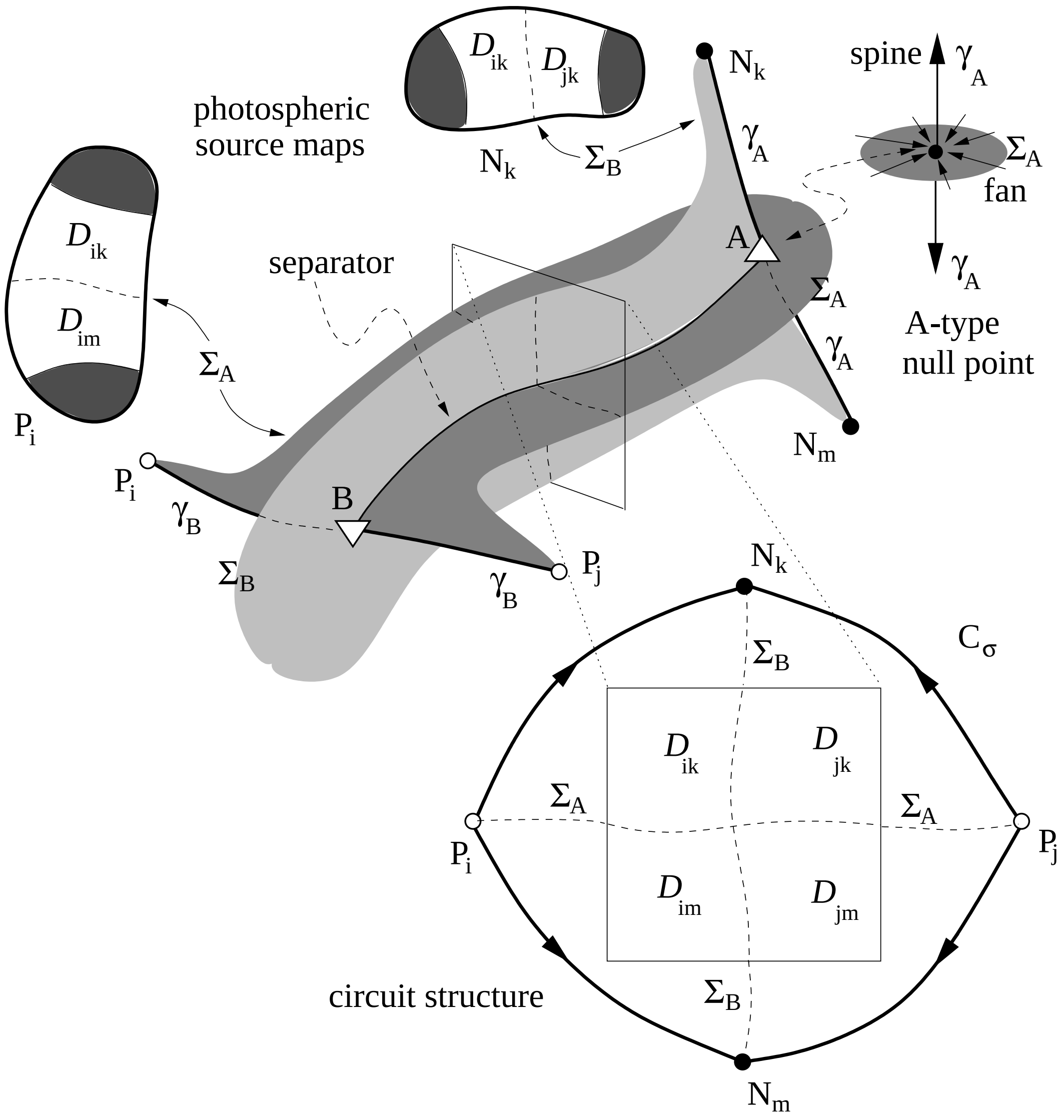

Figure 11. A separator in a three dimensional field. Null points A and B (triangles) have fan surfaces Σ_A and Σ_B shown in grey. These intersect along a single magnetic field line called the separator. Spines from the A-type null connect to negative sources N_k and N_m while spines from the B-type null connect to positive sources P_i and P_j. The separatrix Σ_B is mapped onto the negative source N_k where it separates domains $\mathcal{D}_{ik}$ from domain $\mathcal{D}_{jk}$ as shown in the "photospheric source map". A square membrane is intersected by both separatrices as shown in the "circuit structure" inset. The circuit $\mathcal{C}_\sigma$ encloses only the four domains and is topologically equivalent to the circuit from the two dimensional example fig. 7.

domain graph: $P_i \to N_k \to P_j \to N_m \to P_i$. Only these four domains cross any membrane $\mathcal{M}$ whose boundary is built from circuit field lines. The domains will intersect the membrane in four regions forming the same X-type pattern as fig. 7a in the two-dimensional case. At least one isolating loop, $\mathcal{Q}_\sigma$, will link $\mathcal{C}_\sigma$, and must therefore cross $\mathcal{M}$. The isolating loop will cross $\mathcal{M}$ within one of the separatrices Σ_A or Σ_B.

We are now in a position to analyze an equivalently connected non-potential magnetic field. This will contain the same 4-circuit $\mathcal{C}_\sigma$ bounding a topologically equivalent membrane $\mathcal{M}$. The four contiguous domains will cross the membrane in either of the generic patterns 7b or 7c. Each of these contain a segment R in addition to the separatrices Σ_A and Σ_B. This segment comes from an annular piece of the isolating sheet $\mathcal{S}_\sigma$ called a *current ribbon* [18]. The general magnetic field, (23), contains surface currents on each of the isolating sheets, including this annular ribbon. *This proves that there will, in general, be current ribbons at locations topologically equivalent to each and every separator in the potential field.*

In the two-dimensional case it was possible to demonstrate that no current could flow on the separatrices Σ_A or Σ_B. In the fully three-dimensional case it is harder to make such a categorical statement. A similar argument shows the kinematic difficulty of reconciling a Σ_A or Σ_B separatrix with a surface current in force-balance. The annular sheet defined by e.g. Σ_A will have one edge at the photospheric source P_i (see fig. 11). The edge will lie along the photosphere and the current must flow parallel to the edge, as shown in §3. If this were so then the normal component of the magnetic field, $f(x, y)$, would be discontinuous there. We have assumed each distribution to be continuous so this is impossible. It might be possible that the current density vanishes at the edge of the sheet Σ_A and is non-zero within the interior. It is difficult to see how this sheet-edge might lie within a separatrix and satisfy week force balance, but it is difficult to prove it impossible

5.1 An example

We conclude with a three-dimensional example with non-trivial connections. A potential field with the domain graph fig. 2b is produced using six point magnetic charges placed on $z = 0$. This field has two A-type nulls and two B-type nulls, all in the plane $z = 0$ as shown in fig. 12. The spines of the nulls (solid lines) trace to the source pairs $N4/N6$ (A_1), $N4/N5$ (A_2), $P1/P2$ (B_1) and $P2/P3$ (B_2). Those separatrix field lines lying in the $z = 0$ plane are shown as dashed lines. These two sets of curves delineate the regions where domains intersect the $z = 0$ surface, called their footprint [28]. All seven of the domains intersect the photosphere, so the map may be compared to the domain graph 2b.

The domain graph contains two 4-circuits, $\mathcal{C}_1$ and $\mathcal{C}_2$, corresponding to two separators in the potential field. Circuit $\mathcal{C}_1$ corresponds to a separator linking A_1 to B_2. The isolating loop for this circuit, $\mathcal{Q}_1$, enclosing the chord domain $\mathcal{D}_{34}$, is the

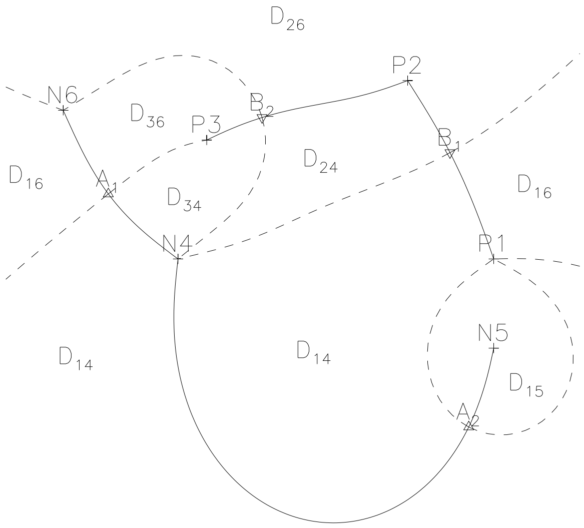

Figure 12. A potential magnetic field with the topology of 2b. Point sources (+) are located on the $z = 0$ plane. Four magnetic nulls (triangle) are also located on his plane. Their spines are traced in solid lines and the photospheric separatrix field lines are dashed. The photospheric portion of each domain is labeled.

same curve shown in fig. 4. The second circuit, $\mathcal{C}_2$, corresponds to a separator linking null B_1 to A_1. An isolating loop can be formed from the separator and some path through the photosphere, however, no possible photospheric path will isolate a single chord domain. If the path $\mathcal{Q}_2$ also incorporates the first separator from A_1 to B_2 and then passes from B_2 to B_1 along the photosphere, it can be made to isolate the chord domain $\mathcal{D}_{24}$ identified in fig. 3. A more natural loop, passing through the photosphere directly from B_1 and A_1, encloses both domains $\mathcal{D}_{34}$ and $\mathcal{D}_{24}$. Either choice produces a loop vector $\vec{\mathcal{Q}}_2$ which is linearly independent of $\vec{\mathcal{Q}}_1$ and is therefore admissible. Using the second choice the isolating fluxes are

$$\Psi_1 = \psi_{34} \quad , \quad \Psi_2 = \psi_{34} + \psi_{24} \quad . \tag{43}$$

Furthermore, either choice of isolating loop $\mathcal{Q}_2$ includes the same section of coronal path, along the separator from A_1 to B_2 where the minimizing field must have a current sheet. The photospheric portion of the path, and portions including previous separators, merely predict current sheets in places already known to have them. Therefore, the structure of the minimizing field is unaffected by the choice of isolating path, beyond the requirement that it link the loop $\mathcal{C}_2$.

The topology has been characterized for a potential magnetic field, but it will not be altered if the system is changed by e.g. moving the photospheric sources. The non-potential equilibrium will contain currents along two sheets which are topologically equivalent to the vacuum separators. Figure 13 shows the geometry of a ribbon related to $\mathcal{Q}_1$. The orientation shown is for the case $\Psi_1 < \Psi_1^{(\mathrm{v})}$ in which current flows from A_1 to B_2. The sheet has a generally vertical orientation near its top, similar to fig. 8b, but without symmetry.

6 Discussion

We have found equations for the a minimum energy magnetic field subject to boundary conditions at $z = 0$. The chief assumption made about the photospheric boundary condition, $f(x, y)$, was that it consisted of isolated unipolar regions. While this is not the most general type of boundary condition, it seems to reflect observations of the solar photosphere.

The new element of this calculation was a constraint on all domain fluxes. This constraint is less restrictive than a constraint on the field-line mapping of the entire photosphere. Since fields which preserve a given field line mapping automatically satisfy the domain flux constraint, the energy of the equilibrium field found here is a lower bound to that of the general force free solution.

The domain-flux-constrained field had two general features: all flux domains are current-free and current sheets occur along certain separatrix surfaces. In two-dimensions there is one current sheet associated with each X-type neutral point in the equivalent potential field. This fact had been previously established using several different lines of argument, none of which could be generalized to three dimensions

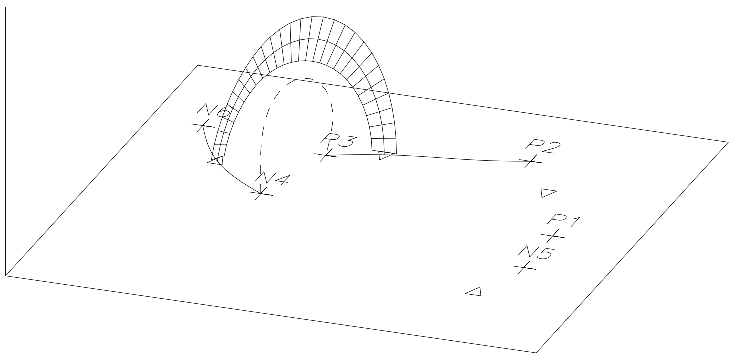

Figure 13. A rendering, using square regions, of a current ribbon along isolating loop $\mathcal{Q}_1$. All sources and nulls are shown on the $z = 0$ plane. The spines from A_1 and B_1 are shown as solid lines. A coronal field line from domain $\mathcal{D}_{34}$ is shown as a dashed line.

[8, 9, 10]. Moreover, a general formalism for calculating general fields of this kind, called quasi-singular potential fields, has been developed following different motivation [11, 24].

Our calculation applies equally to three dimensions, where the sheets are current ribbons. We have shown that there is one current ribbon associated with each separator in the equivalent potential field. This result had been anticipated [18], since a separator is the analog of an X-type neutral point in two-dimensional potential fields. Its applicability to fields of arbitrary geometry makes it a powerful tool in the analysis of solar observations [29, 30]. The above calculation provides the theoretical framework on which such modeling can be based.

There has been some debate as to whether discontinuous equilibria are consistent with a spatially continuous footpoint mapping [3, 31, 32, 33, 12]. It is generally accepted, however, that they are consistent with discontinuous footpoint mappings [34]. While our photospheric boundary field $f(x, y)$ might be continuous its footpoint mapping will certainly be discontinuous; regions where $f(x, y) = 0$ have no mapping. For this reason it is not surprising that the resulting equilibrium contains current sheets.

The fact that current sheets are present in a state of minimum magnetic energy demonstrates that they are stable under ideal MHD evolution. An equilibrium is unstable if the variation of its energy can be negative for some allowed perturbations [35]. A minimum in our flux-constrained system cannot be energetically decreased by any change which preserves domain fluxes. Since these are a super-set of ideal, line-tied perturbations, the equilibrium must be ideally stale. While we have not rigorously proven that a minimum exists within the set of allowed fields, it seems plausible since the set is not empty (connect the domains with isolated flux bundles) and the energy is bounded from below. If a minimum energy does exist it must satisfy the Euler-Lagrange equations which include current sheets between domains, regardless of how complex the photospheric field.

Every domain in the minimizing field is current-free, owing to the unrestrictive nature of our constraints. A distributed current would result from field lines twisted about each other within a domain. Without full line-tying constraints, it is always possible to untwist the footpoints of these lines, thereby reducing the overall energy.

It is conceptually useful to recover the more restrictive line-tying constraints as a limit of flux-domain constraints. The limit is approached by recursively dividing each source region into sub-regions, and constraining the fluxes in the resulting sub-domains. In the limit of infinitesimal sub-regions the domain-flux constraints become line-tying constraints. Upon division, the old domains become filled with separatrices along which current may flow; in the limit this becomes a distributed current. Since this procedure increases the number of constraints, it will naturally raise the energy of the minimizing field. In the limit this is the general force-free equilibrium, whose energy we have shown is always greater than the flux-constrained equilibrium,

Flux-constrained equilibria provide a simpler, N_c-dimensional, space in which to study the energetics of complex fields. For given boundary data $f(x,y)$ the free magnetic energy depends only on the flux differences $\Delta\Psi_\sigma$. One example is the energetics of separator reconnection [16, 17]. If flux is reconnected at a rate $\dot{\psi}$, the domain-flux vector will change according to its circuit-vector

$$\frac{d\Delta\Psi_\sigma}{dt} \;=\; \frac{d}{dt}\left(\vec{\mathcal{Q}}_\sigma\cdot\vec{\psi}\right) \;=\; \vec{\mathcal{Q}}_\sigma\cdot(\dot{\psi}\vec{\mathcal{C}}_\sigma) \;=\; \dot{\psi} \quad . \tag{44}$$

This leads immediately to a relation between the flux-transfer and the energy release due to magnetic reconnection

$$\frac{d\Delta W}{dt} \;=\; \frac{\partial\Delta W}{\partial\Delta\Psi_\sigma}\,\dot{\psi} \;=\; I_\sigma\,\dot{\psi} \quad , \tag{45}$$

using equation (32). This provides a lower bound on the energy release rate in a full MHD calculation since, ΔW is lower bound on the free energy.

A separate application of the model is an estimate the energy supplied to the coronal field by photospheric motion. Photospheric motion changes the boundary field $f(x,y)$, thereby changing the potential field $\mathbf{B}^{(\mathrm{v})}$ and the potential fluxes $\Psi_\sigma^{(\mathrm{v})}$. Under ideal evolution, the domain fluxes would not change during evolution. Thus Ψ_σ would be constant, but $\Delta\Psi_\sigma$ would change due to changes in $\Psi_\sigma^{(\mathrm{v})}$. This will result in changes to the free energy ΔW and to the potential-field energy. The Poynting flux through the photosphere will be the sum of these changes, however, it is likely that only the injection of free energy is available for coronal heating.

Acknowledgments

The author wishes to acknowledge discussions with Dr. I. Klapper, Dr. B.C. Low. This material is based upon work supported by the National Science Foundation under grant No. ATM-9733424.

References

[1] E. R. Priest, *Solar Magnetohydrodynamics*, volume 21, D. Reidel, Boston, 1982.

[2] B. A. Hagyard, M. Stark and P. Venkatakrishnan, Solar Phys. **184**, 133 (1999).

[3] E. N. Parker, ApJ **174**, 499 (1972).

[4] R. H. Levine, ApJ **190**, 457 (1974).

[5] P. A. Sweet, in *Electromagnetic Phenomena in Cosmical Physics*, edited by B. Lehnert, Cambridge University Press, Cambridge, U.K., 1958, pp. 123–134.

[6] E. R. Priest, Rep. Prog. Phys. **48**, 955 (1985).

[7] E. N. Parker, ApJ **264**, 642 (1983).

[8] R. M. Green, Modes of annihilation and reconnection in magnetic fields, in *Stellar and Solar magnetic fields. Proc. IAU Symp. 22*, edited by R. Lust, pp. 398–404, North-Holland, 1965.

[9] S. I. Syrovatskii, Sov. Phys. JETP **33**, 933 (1971).

[10] E. R. Priest and M. A. Raadu, Solar Phys. **43**, 177 (1975).

[11] J. J. Aly and T. Amari, A&A **221**, 287 (1989).

[12] E. N. Parker, *Spontaneous current sheets in magnetic fields : with applications to stellar x-rays*, Oxford University Press, 1994.

[13] V. S. Gorbachev and B. V. Somov, Solar Phys. **117**, 77 (1988).

[14] D. W. Longcope, Solar Phys. **169**, 91 (1996).

[15] C. Zwaan, ARA&A **25**, 83 (1987).

[16] J. M. Greene, JGR **93**, 8583 (1988).

[17] Y.-T. Lau and J. M. Finn, ApJ **350**, 672 (1990).

[18] D. W. Longcope and S. C. Cowley, Phys. Plasmas **3**, 2885 (1996).

[19] S. Seshu and M. B. Reed, *Linear Graphs and Electrical Networks*, Addison-Wesley, Reading, MA, 1961.

[20] S. C. Cowley, D. W. Longcope, and R. N. Sudan, Physics Reports **283**, 227 (1997).

[21] I. J. D. Craig, A&A **283**, 331 (1994).

[22] Y. Q. Hu and B. C. Low, Solar Phys. **81**, 107 (1982).

[23] N. I. Muskhelishvili, *Singular Integral Equations*, Dover, New York, 1992.

[24] V. S. Titov, Solar Phys. **139**, 401 (1992).

[25] T. N. Bungey, V. S. Titov, and E. R. Priest, A&A **308**, 233 (1996).

[26] S. W. H. Cowley, Radio Sci. **8**, 903 (1973).

[27] J. M. Parnell, C. E.and Smith, T. Neukirch, and E. R. Priest, Phys. Plasmas **3**, 759 (1996).

[28] B. T. Welsch and D. W. Longcope, ApJ **522** (1999).

[29] D. W. Longcope and A. V. R. Silva, Solar Phys. **179**, 349 (1998).

[30] C. C. Kankelborg and D. W. Longcope, Solar Phys. **190**, 59 (1999).

[31] A. A. Van Ballegooijen, ApJ **298**, 421 (1985).

[32] S. K. Antiochos, ApJ **312**, 886 (1987).

[33] D. W. Longcope and H. R. Strauss, ApJ **437**, 851 (1994).

[34] B. C. Low, ApJ **323**, 358 (1987).

[35] I. B. Bernstein, E. A. Frieman, M. D. Kruskal, and R. M. Kulsrud, Proc. Roy. Soc. Lond. **A244**, 17 (1958).